Chemical Engineering Journal 434 (2022) 134665

Contents lists available at ScienceDirect

Chemical Engineering Journal

journal homepage: www.elsevier.com/locate/cej

Function transformation of polymeric films through morphing of surface shapes

Hyemin Lee [a,1], Yoon Ji Seo [a,1], Jaekyoung Kim [d], Myung Jun Bae [a], Seokhoon Hwang [a], Jung Gun Bae [b], Won Bo Lee [b], Hyunsik Yoon [a,c,d,*]

[a] Department of Chemical and Biomolecular Engineering, Seoul National University of Science and Technology, Seoul 01811, Republic of Korea
[b] School of Chemical and Biological Engineering, Seoul National University, Seoul 08826, Republic of Korea
[c] Department of Nano and Bioengineering, Seoul National University of Science and Technology, Seoul 01811, Republic of Korea
[d] Department of New Energy Engineering, Seoul National University of Science and Technology, Seoul 01811, Republic of Korea

ARTICLE INFO

Keywords:
Function transformation
Shape morphing
Hydrogels
Wetting
Films

ABSTRACT

The functions of materials are correlated with their shapes. Here, we propose a scheme of functional transformation of a polymeric film by changing the surface shape. After the preparation of straight shapes such as lines or rectangles on a substrate by conventional microfabrication methods, we transformed the shapes into laterally buckled or inversely tapered shapes. The change in surface shape induced stress dissipation or superomniphobic functions, which are difficult to obtain with straight shapes. To transform the shapes, we harnessed a method of swelling hydrogel shapes bonded to a substrate. We replicated the swollen shapes with functional materials by photopolymerization of liquid prepolymers filled within the cavities of the swollen hydrogel shapes. We investigated methods to hold water molecules within the hydrogel networks during photopolymerization by controlling the surface energy of the photocurable liquid prepolymer and removing air between the liquid prepolymer and the cavities for easy infiltration of the liquid prepolymer into the inversely tapered shapes. The proposed scheme of function transformation by using surface shape morphing can be a platform technology for developing unprecedented functions depending on shape.

1. Introduction

The physical function of a material is correlated with its dimension or shape. Silicon is a hard material with a high Young's modulus, but it can be flexible when the thickness is less than tens of nanometers [1]. Metal is a reflective material, but it can show color when it has a submicron grating shape [2]. SiO_2 is a hydrophilic material, but it can be superhydrophobic if it has the shape of doubly re-entrant structures [3]. Given this background, many researchers have studied special functions related to unique shapes [4–11]. Materials with multiscale surface roughness show functions of water repellency or beautiful color; asymmetric shapes induce directional liquid movement, which can be used for water harvesting; and the three-dimensional (3D) suction cup shape has a high adhesion function even in water. To exploit special shapes, especially at the microscale, microfabrication methods such as photolithography have been used to fabricate microarrays with special shapes on the surface of a film. However, the conventional method can provide only two-dimensional (2D) shapes because light-induced photolithography uses a mask and ultraviolet (UV) light exposure to crosslink or change the chemistry of a 2D film coated on a flat substrate [12]. Although two-photon lithography and 3D printing have been developed to construct complicated 3D-shaped features, issues of low throughput or low resolution remain [13,14]. To obtain unique 3D shapes on a surface, we have considered shape morphing approaches for changing 2D to 3D shapes by using hydrogel swelling under constrained conditions. The study of shape morphing schemes has been inspired by biological systems such as pine cones and wheat awns, which show deformation under hydration and dehydration. Therefore, hydrogel materials have been extensively used for research on shape morphing [15–30]. Hydrogel materials can be swollen under humid conditions or in water due to the interpenetration of water molecules within the hydrogel networks. They have received attention because the swelling

* Corresponding author at: Department of Chemical & Biomolecular Engineering, Seoul National University of Science & Technology, Seoul 01811, Republic of Korea.
E-mail address: hsyoon@seoultech.ac.kr (H. Yoon).
[1] These authors contribute equally to this work.

https://doi.org/10.1016/j.cej.2022.134665
Received 30 October 2021; Received in revised form 21 December 2021; Accepted 9 January 2022
Available online 13 January 2022
1385-8947/

behavior can be controlled by the crosslinking density and external signals such as pH and temperature [15–19]. Researchers have modified the deformation of hydrogel shapes by using volume expansion in constrained conditions during swelling. For instance, bending of bilayer systems with hydrogels with different swelling degrees [20–22], out-of-plane deformation of in-plane hydrogel sheets by spatial control of hydrogel crosslinking densities [23–26], deformation of hydrogel shapes fabricated by 3D printing [27], and creation of creases by the swelling of hydrogel structures constrained by microfabricated patterns have been used for biomimetic applications, soft robotics, and biomedical applications [28–30]. Although shape morphing by hydrogels has the advantages of reversible changes and various inputs, hydrogel materials are too soft to be used in mechanical applications, and they are hydrophilic themselves and cannot be used for producing liquid-repellent surfaces. In addition, the application of 3D hydrogel shapes is limited to use in water or humid conditions.

In this work, we propose a scheme of function transformation based on morphing straight hydrogel shapes on a film surface by swelling hydrogel structures bonded to a substrate and replicating the shapes by using functional materials. Due to local volume expansion under constrained conditions, rectangular pillar shapes are transformed into inversely tapered shapes, and line shapes are transformed into laterally buckled shapes. To utilize special functions arising from the transformed shapes, we replicated the swollen hydrogel shapes with functional materials while water was held within the hydrogel networks. To maintain the swollen shapes during replication, we first used photopolymerization with a fluorinated liquid prepolymer. The hydrophobic property of the fluorinated polymer prohibits the movement of water molecules in the hydrogel networks during photopolymerization. Second, we controlled the infiltration of the hydrophobic photocurable liquid prepolymer into the narrowed entrances of the swollen hydrogel structures by implementing vacuum conditions. The transformed shapes, such as inversely tapered shapes in a fluorinated material or laterally buckled shapes in an elastomeric material, can be used for practical applications of superomniphobic or stress-dissipating films. This film function transformation scheme based on the replication of swollen hydrogel shapes by functional materials can be a platform technology for creating unprecedented functions originating from the unique shapes produced.

2. Results and discussion

Fig. 1A and B shows the shape and function transformation scheme. In this work, we used arrays with straight-line (Fig. 1A) and rectangular shapes (Fig. 1B) fabricated on a film surface and transformed the shapes into laterally buckled lines and an inversely tapered shapes,

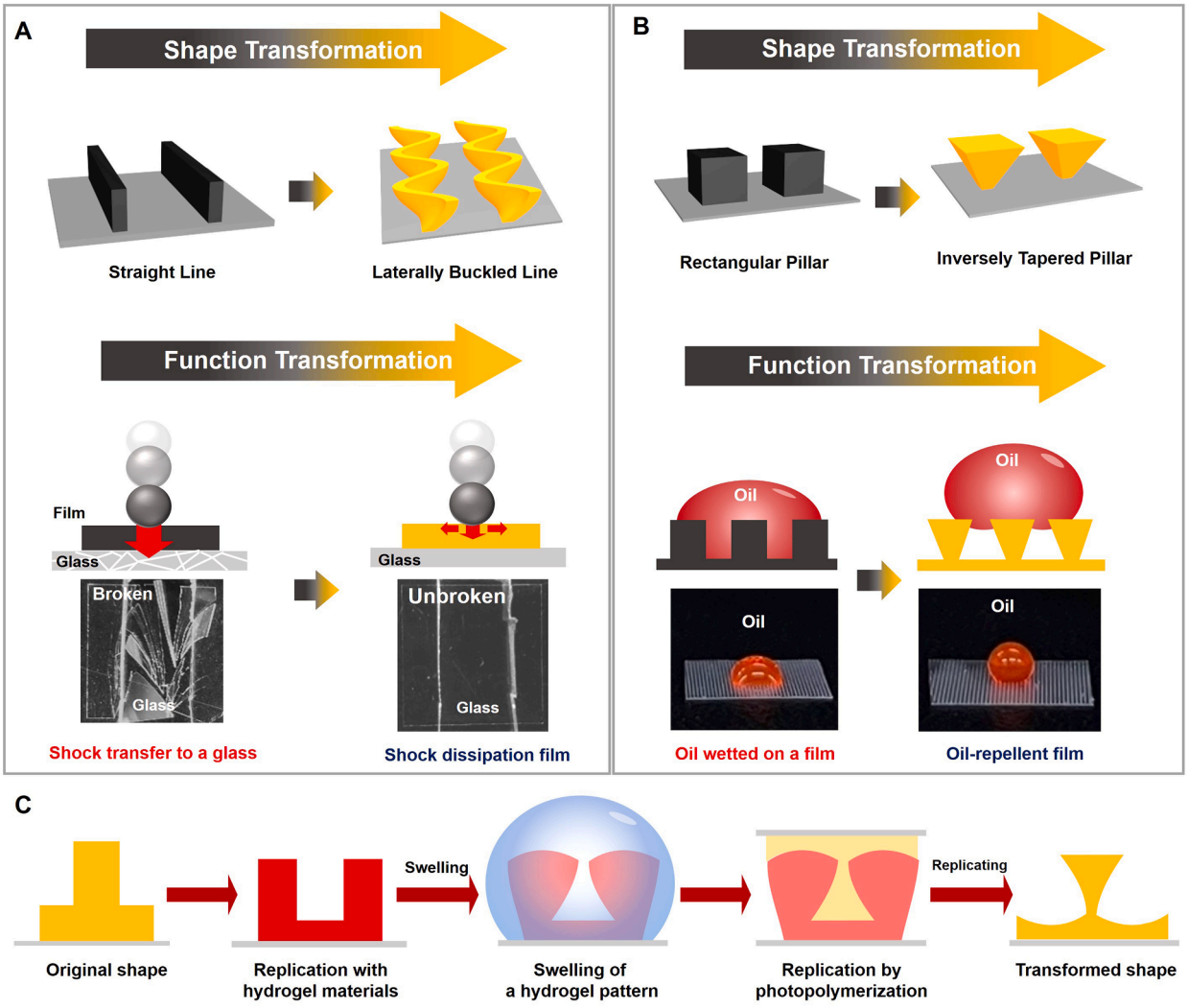

Fig. 1. (A) Schematic illustration of the shape and function transformation of straight-line structures. A film transferring stress to thin glass is transformed into a stress-dissipating film. (B) Schematic illustration of the shape and function transformation of a rectangular pillar shape. An oil-wetting surface is transformed into an oil-repellent surface. (C) Scheme of the experimental procedure for shape transformation with hydrogel swelling.

respectively, by local volume expansion under a constraint imposed by bonding to a substrate. The top areas of the lines buckle due to volume expansion in the top areas and constraint in the bottom areas [31–36]. In the case of rectangular patterns, the recessed patterns swell, and the unrestricted regions at the entrances of holes swell more than the restricted bottom regions. Because the function of a film is dependent on its shape, films can have different functions even if they are made of the same materials. In the case of a film with straight line shapes on the surface, a normal force applied on the film is transferred to the glass substrate underneath it. The transformed shapes exhibit lateral buckling; the normal stress is dissipated, and the glass underneath is protected. As a second example, a film with a rectangular shape on the surface can be wetted by a low-surface-energy liquid because Laplace pressure is applied to the bottom. After transformation to an inversely tapered structure, however, this film shows oleophobicity because the shape maintains the Cassie state by holding air within its cavities. Although we have shown two examples, we note that the function transformation scheme can be extended to various geometric structures for various functions. Fig. 1C shows a schematic illustration of the experimental procedure. First, we prepared original masters by using conventional microfabrication methods such as photolithography or soft lithography. Then, we replicated the shapes with hydrogel materials by using photopolymerization. After preparing straight hydrogel structures attached to a polyethylene terephthalate (PET) film, we exposed the film to a water environment. The water molecules interpenetrated into the hydrophilic hydrogel networks, and the microscale hydrogel structures swelled. In this work, we used hydroxyethyl methacrylate (HEMA) as a base hydrogel and added additives to control the swelling ratio. The swollen 3D shapes were determined by the geometrical constraint and the swelling ratio. To replicate the swollen shapes with other functional materials, we filled photocurable liquid prepolymers within the cavities of the swollen hydrogel structures and solidified the liquid prepolymers by using photopolymerization. The swollen hydrogel structure was easily separated from the solidified prepolymer due to the elasticity of the hydrogel [37]. To hold water molecules within the hydrogel network during photopolymerization, we optimized the experimental conditions. Inversely tapered shapes with fluorinated polymers were fabricated to realize a repellent function for low-surface-energy liquids, and laterally buckled shapes made of an elastomer were fabricated to realize a stress dissipation function. (More details of the fabrication process and optical microscope images are provided in the experimental section and in Figs. S1-S4). Another advantage of the method is the versatility in the choice of materials. We replicated the initial replicated patterns again with conventional polymers, such as polystyrene (PS), obtaining 3D shapes of the swollen hydrogels. Fig. S5 shows the results of double replication of 3D morphed shapes with PS, polyurethane acrylate (PUA) [38,39], and perfluoropolyether (PFPE) [40,41] through shape transformation. We fabricated inversely tapered and laterally buckled structures with three different UV-curable (PUA 301, PUA 311, PFPE) and thermoplastic (PS) polymers via soft lithography and thermal imprinting. We note that replication from complicated 3D shapes was possible due to the softness of the swollen hydrogels or polydimethylsiloxane (PDMS) [42].

To polymerize a liquid prepolymer filled within the cavities of a swollen hydrogel surface, we investigated several experimental parameters. Fig. 2A shows two possible results of the polymerization of liquid prepolymers within swollen hydrogel cavities. If the liquid prepolymer is hydrophilic, then water molecules within the hydrogel network can move to the liquid prepolymer during polymerization, and the swollen hydrogel shape can return to the original shape (upper part of Fig. 2A). In contrast, if the liquid prepolymer has a low affinity for water, then the hydrogel network can hold water during photopolymerization of the hydrophobic prepolymer. Therefore, selecting a liquid prepolymer that has a lower affinity than the hydrogel for water is essential. In this work, we used three different prepolymers (PFPE, PUA and polyethylene glycol diacrylate (PEGDA)) to observe the effect of their affinity for water. After obtaining the inverse shapes of the swollen hydrogel shapes by photopolymerization, we fabricated double-replicated PDMS patterns to observe the swollen hydrogel shapes. Fig. 2B shows scanning electron microscopy (SEM) images of PDMS shapes replicated from inverse shapes with PFPE, PUA, and PEGDA polymerized in the swollen hydrogel shapes. When we used PFPE, water remained in the hydrogel during the photopolymerization process because the fluorinated group has a low surface energy and a low affinity for water, and laterally buckled shapes were maintained. In contrast, when we used PUA, the water in the hydrogel network moved to the PUA prepolymer during photopolymerization, and the buckled hydrogel structures tended to return to their original line shapes during replication. This behavior occurred because the liquid PUA prepolymer has a higher affinity than the fluorinated liquid prepolymer for water. Notably, when we used PEGDA as a liquid prepolymer, it bonded to the hydrogel during photopolymerization due to the high adhesion between PEGDA and HEMA.

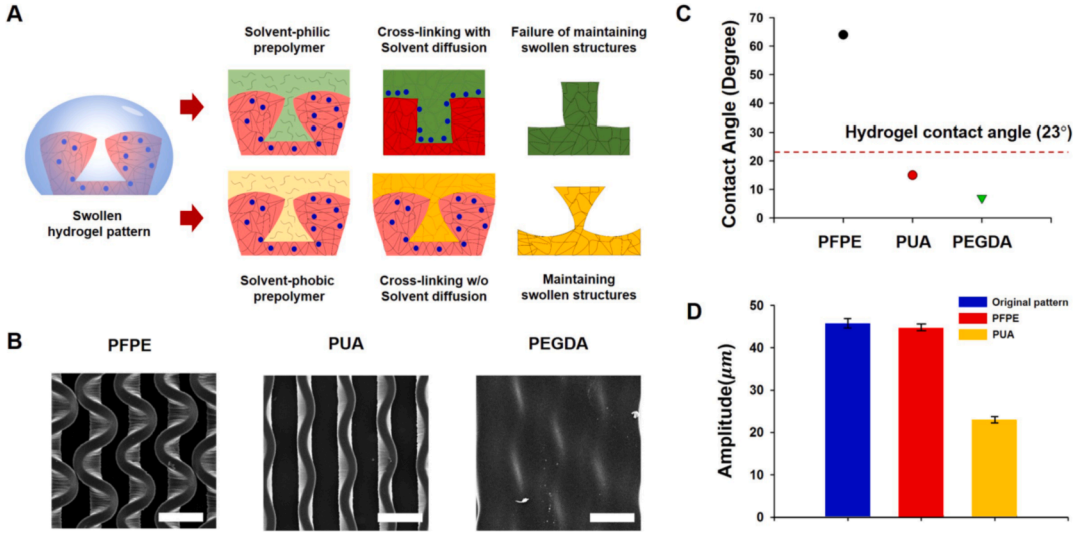

Fig. 2. (A) Schematic illustration of photopolymerization with hydrophilic and hydrophobic liquid prepolymers filled into swollen hydrogel shapes. (B) SEM images of structures doubly replicated from initial replicated shapes by photopolymerization with different liquid prepolymers (PFPE, PUA, and PEGDA) in swollen hydrogel patterns. Scale bars are 50 μm. (C) Graph of the contact angles of water on different liquid prepolymers. (D) Graph of the amplitudes of laterally buckled structures for original hydrogel structures and doubly replicated structures. Scale bars are 50 μm.

To quantitatively compare the affinities for water of the liquid prepolymers and the swollen hydrogel mold, we measured the contact angles of water on the liquid prepolymers (Fig. 2C). We prepared a flat swollen hydrogel film (by dropping a water droplet on a cured hydrogel film) and flat films coated with liquid prepolymers, and then, we dropped a water droplet on each of the films and measured the contact angle. The contact angle of water on the swollen hydrogel film was 23°. The contact angles of water on the PUA and PEGDA liquid prepolymers were lower (17° and 7°, respectively) than that on the hydrogel film (pictures of the contact angles can be seen in Fig. S6). This result indicates that the liquid prepolymers PUA and PEGDA have a higher water affinity than the swollen hydrogel networks. In contrast, the contact angle for the fluorinated liquid prepolymer (PFPE) was 64°, which is much higher than that for the swollen hydrogel film. This result indicates that the water affinity of PFPE is lower than that of the hydrogel, so the swollen shape of the hydrogel can be maintained during photopolymerization. To confirm the degree of recovery from deformation, we compared the shape changes over time in the liquid prepolymers (PFPE, PUA, and PEGDA). We covered the swollen buckling structures with prepolymers and kept them for 30 s, 1 min, and 5 min. The swollen structure was maintained when it was covered with PFPE, but in the case of PUA and PEGDA, the shape recovered over time (Fig. S7). Additionally, we measured the buckling amplitudes of the replication patterns and compared them with the original buckling amplitude (swollen hydrogel). The buckling amplitude of PUA (~23 μm) was lower than that of PFPE (~44 μm), which was similar to the original amplitude (~46 μm) (Fig. 2D).

When obtaining inversely tapered shapes from swollen hydrogel patterns, the trapped air between the liquid prepolymer and the cavities can be critical for infiltration. Recently, re-entrant structure surfaces were studied for their oleophobicity because liquids can float on the air trapped in re-entrant structures [43–47]. To remove the air trapped within cavities, an external force such as pumping must be applied to produce a vacuum condition. After covering liquid prepolymer on the re-entrant structures formed by hydrogel swelling, we evacuated the trapped air to the top surface of the liquid for several seconds, as shown in Fig. 3A. Then, we removed the air bubbles on the top surface of the liquid and placed a PET film on the liquid prepolymer. The liquid prepolymer that had infiltrated into the cavities was crosslinked by photopolymerization. Fig. 3B shows the result of replication without pumping to remove trapped air. The areas with trapped air are not filled with the liquid prepolymer, and we only obtained crosslinked polymers in the entrance region. In contrast, when we removed the trapped air from the cavities of the re-entrant structures, we obtained whole inversely tapered shapes. To control the removal rate of trapped air from the cavities, we controlled the vacuum conditions as well as the surface tension of the liquid prepolymer (PFPE = 19 mN/m, PUA301 = 31 mN/m, RS1550R = 43 mN/m). We pumped swollen hydrogel patterns covered with liquid prepolymer after placing them in a vacuum chamber (SH-VDO-30NG; vacuum range from 0.01 to 1 bar) and stopped pumping immediately when the pressure reached the target vacuum condition. We note that the swollen hydrogel shapes returned to their original shapes when the vacuum time was over 1 h due to the evaporation of water molecules inside the hydrogel networks (Fig. S8).

Fig. 3C shows a graph and SEM images of samples replicated from swollen hydrogel patterns under different conditions. Under atmospheric pressure, only the liquid prepolymer at the entrance of the hydrogel patterns was polymerized because the liquid could not infiltrate into the cavities of the hydrogel patterns. When we decreased the pressure, the liquid prepolymer started to infiltrate into the cavities through the removal of trapped air. When using a liquid prepolymer with a low surface tension (PFPE), the liquid infiltrated when the pressure difference reached 0.25 bar. For the higher-surface tension liquid (RS1550R), air trapped within the cavities was not removed, although the liquid wetted all the surfaces of the swollen hydrogel patterns. With a high-surface tension liquid, the vacuum level must be higher to remove air trapped within cavities. SEM images of all conditions can be seen in Fig. S9. Liquid prepolymer coated on hydrogel patterns can enter cavities when the pressure difference is greater than the breakthrough pressure, which is expressed as follows [43]:

$$P_{break} \sim 2\sigma/x$$

where σ represents the surface tension of the liquid prepolymer and × represents the width of the cavity entrance. This relationship indicates that we need external pressure to remove the air inside the cavities, and the breakthrough pressure is proportional to the surface tension of the liquid prepolymer, which is in good agreement with the experimental results.

To exploit the shapes transformed from rectangular shapes, first, we used the film with inversely tapered shapes on the surface as an oil-repellent film. The inversely tapered shapes prepared by photopolymerization within swollen hydrogel structures can be controlled by the swelling ratio of the hydrogel. Hydrogels with three swelling ratios were prepared (1.71, 2.01 and 2.76) by adjusting the ratio of acrylamide (AAm) to HEMA (details of the hydrogel synthesis can be seen in the experimental section). Fig. 4A shows the overall experimental results according to the experimental parameters. As the swelling ratio increased, the straight shapes exhibited more deformation in the entrance region. We measured the taper angles defined in Fig. 4B as a function of the swelling ratio. The taper angle increased with increasing swelling ratio. Oleophobicity is indicated by a taper angle (as defined in Fig. 4B) lower than the intrinsic contact angle of an oil droplet on the surface [44–46]. If the taper angle is higher than the contact angle, Laplace pressure is applied to the bottom, and the oil can wet the film

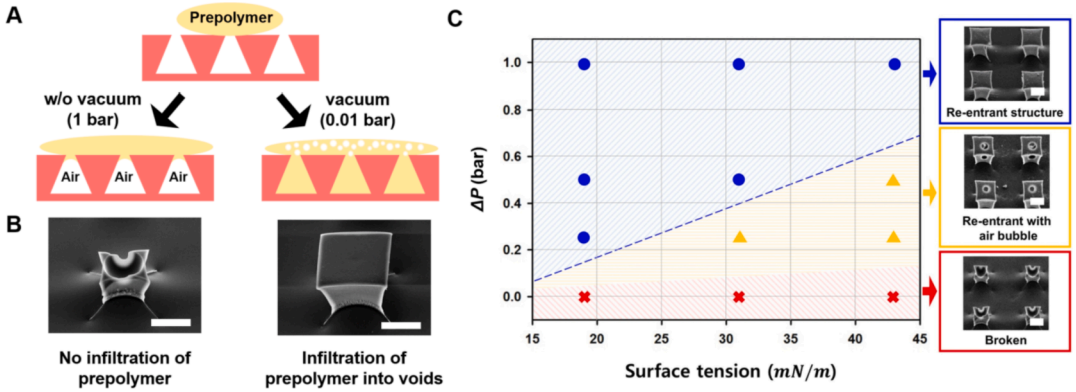

Fig. 3. (A) Schematic illustration of the difference in the infiltration of liquid prepolymer into the air cavities of inversely tapered shapes. (B) SEM images of polymerized polymeric structures without/with vacuum to remove trapped air between the liquid prepolymer and cavities. (C) Graph of the results after photopolymerization of a liquid prepolymer under different vacuum conditions and surface tensions of the liquid prepolymer. Scale bars are 50 μm.

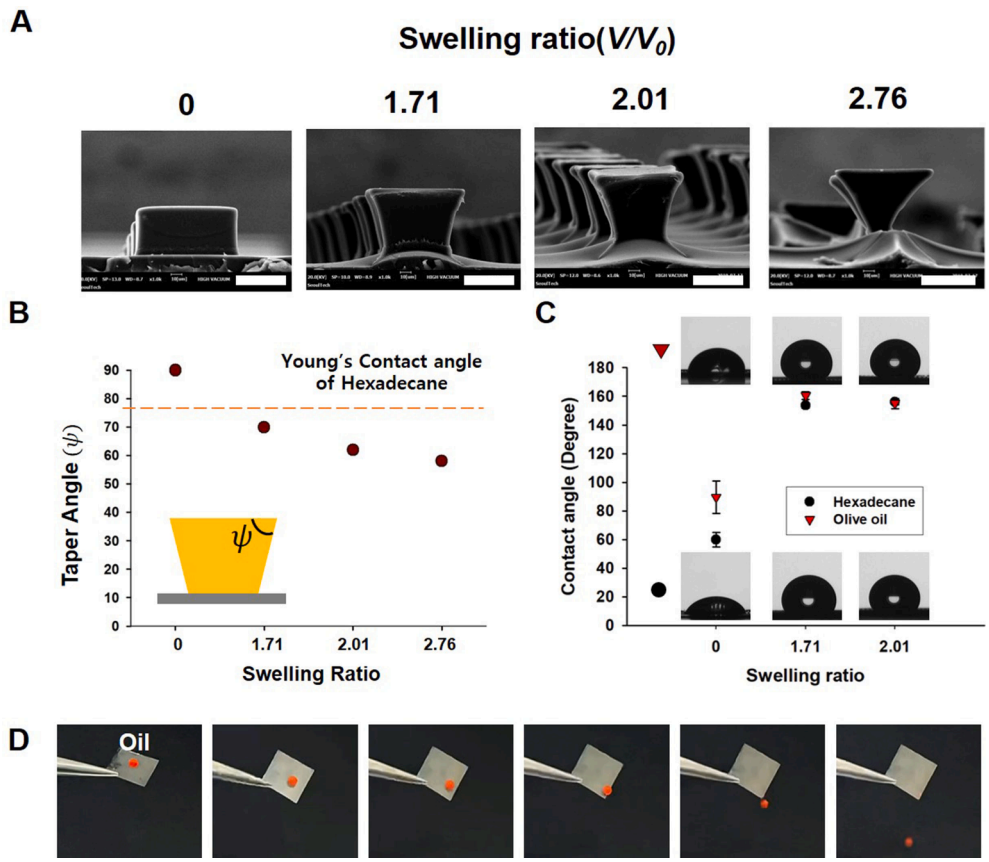

Fig. 4. (A) SEM images of inversely tapered shapes polymerized from swollen hydrogel cavities at different swelling ratios (scale bar = 50 μm). (B) Graph of taper angles according to swelling ratio. (C) Contact angles of hexadecane and olive oil on the surface of samples with inversely tapered shapes. (D) Movie frames of the oil repellency of a film surface with inversely tapered shapes.

surface. In contrast, Laplace pressure is applied upward when the taper angle becomes smaller than the contact angle (Fig. S10). For example, we can predict that the taper angle should be less than 77° for a structure to have a liquid-repelling function because the measured contact angle of hexadecane on the fluorinated material (PFPE) was 77°. In this work, the taper angles of inversely tapered shapes fabricated from hydrogels with swelling ratios of 2.76 (58°), 2.01 (62°) and 1.71 (70°) were lower than the intrinsic contact angle. To confirm our prediction, we dropped olive oil and hexadecane on the structures and measured the contact angle with a contact angle meter (CAM-200, KSV). The contact angle results are shown in the graph of Fig. 4C. The contact angle on the film with inversely tapered shapes on its surface was larger than that on the film with rectangular pillars on its surface, indicating that the inversely tapered shapes are more suitable than the straight shape for making an oleophobic surface. We note that the contact angle is also dependent on the spacing ratio (Fig. S11). To confirm the oleophobic function of the film, we tested the repellency of the surface. The sample used in the experiment was made of a solution with a swelling ratio of 2.01. We placed an olive oil droplet on the film and then tilted the film to repel the oil from the film. Fig. 4D shows movie frames of oil being repelled from the film. We inserted a dye (Nile red) for better demonstration. The experimental results show the possibility of fabricating surfaces that can prevent contamination by organic solvents by transforming rectangular shapes to inversely tapered shapes through replication from swollen hydrogel structures.

Another example of harnessing transformed functions is the use of a film with laterally buckled structures on its surface for stress dissipation. As mobile devices become thinner, a thin film is necessary to absorb external impacts to protect active devices such as organic light-emitting diodes (OLEDs) [48]. We investigated the stress dissipation performance of laterally buckled shapes transformed from line shapes replicated by conventional rubber (PDMS). Fig. 5A shows SEM images of a hydrogel line shape (25 μm in width and 50 μm in height) and the laterally buckled shape (the amplitude of the wavy shape is 50 μm from the center; the swelling ratio is 2.01) transformed from the line shape after double replication. The line shapes are transformed into laterally buckled shapes when they are swollen by water molecules due to the increase in surface area while bonded to a substrate, and the amplitude of lateral buckling can be controlled by the swelling ratio of the hydrogel and the designed line shapes. Fig. S12 shows SEM images of laterally buckled PDMS structures doubly replicated from swollen hydrogel structures. We prepared hydrogel line patterns (25 μm in width and 50 μm in height) and swelled the line patterns by dipping them in a water bath. The amplitude of lateral buckling was 41 μm (B1) and 50 μm (B2) when the swelling ratio was 1.71 and 2.01, respectively. As shown in Fig. S12, the amplitude increased with increasing swelling ratio. The relation between the amplitude of lateral buckling (A) and the swelling strain ($\beta = swelling\ ratio^{1/3}$) was reported to be $A \sim \lambda\beta^{1/2}$, which is in good agreement with our experimental results [31]. We expected a film with a laterally buckled shape embedded on the surface to have a stress dissipation function that protects thin glass beneath the film because the structure is in the form of a lateral spring. To investigate the stress dissipation effect of laterally buckled surface shapes, we prepared films without patterns, with a line pattern, and with laterally buckled patterns in two different amplitudes (B1 and B2) with the same film thickness. Then, we placed a thin glass slide ($t = 150$ μm) on a thick block with an empty center and covered it with the designed stress dissipation films ($t = 1$ mm) made of PDMS. To apply mechanical stress, we dropped a ball (steel, 4 g) from different heights ($h = 10$, 15, 20, 25, 30 and 35 cm) onto glass slides covered by the stress dissipation films. The experimental

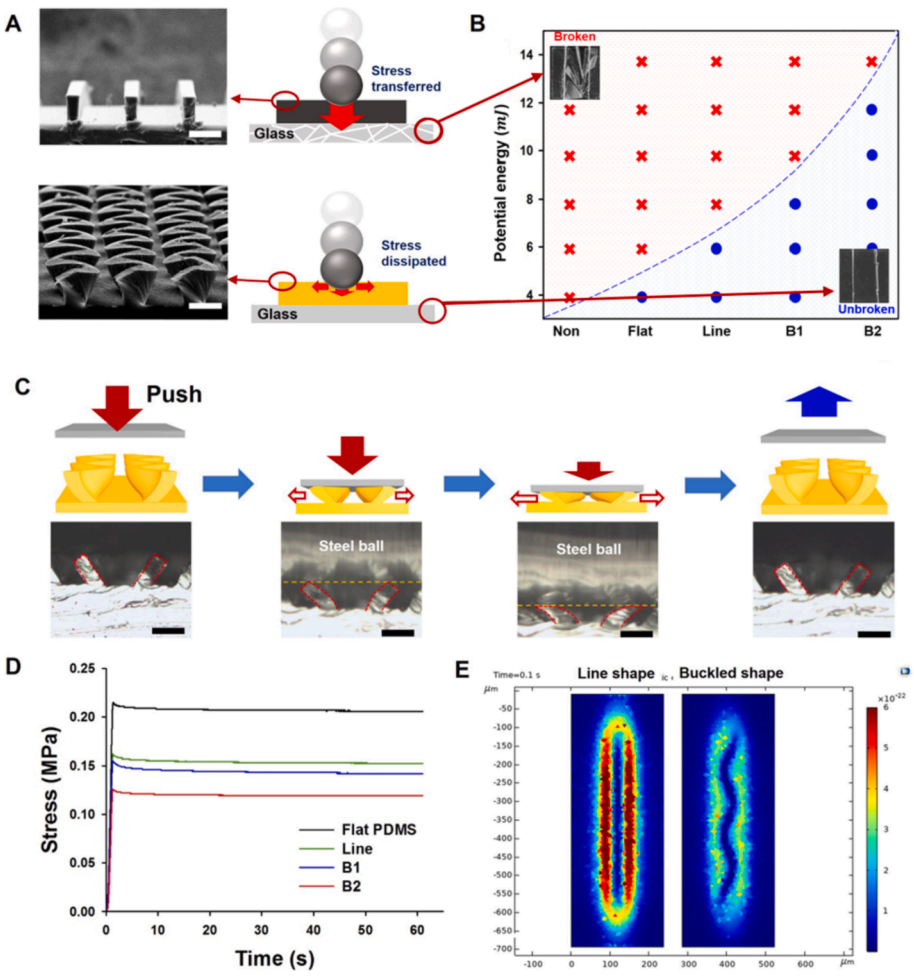

Fig. 5. (A) SEM images of original (line) and laterally buckled shapes obtained by double replication from swollen hydrogel structures (scale bar = 50 μm) and schematic illustration of stress transfer and dissipation through the film. (B) Graph of fracture results showing that the laterally buckled surface has the highest stress dissipation performance. (C) Microscopic pictures of stress release on laterally buckled structures. (D) Stress relaxation curves for the compression of flat, line-patterned films with laterally buckled surface shapes with different amplitudes (41 μm (B1) and 50 μm (B2)). (E) FEM simulation results of the kinetic energy transferred from line patterns and laterally buckled patterns.

setup is shown in Fig. S13. Fig. 5B shows the results of the fracture test. The thin glass was broken by 5.9 mJ and 7.8 mJ when the flat and line-patterned films were tested; however, the glass was not broken until the potential energy reached 11.7 mJ when it was covered by the film with laterally buckled shapes of larger amplitude (B2). The total fracture pictures can be seen in Fig. S14. The fracture test results show that the laterally buckled structure can dissipate the kinetic energy transferred to the substrate below the film and has the potential to protect devices with a glass substrate. Fig. 5C shows microscopic pictures of the deformation of laterally buckled structures when they were compressed with a steel ball (diameter of 10 mm). The laterally buckled line shapes can dissipate normal stress into the lateral direction due to the lateral deformation of the patterns, and the structure recovers when the stress is released because the unique 3D feature of the laterally buckled structures enables them to act as lateral spring structures. To investigate the degree of stress dissipation of the laterally buckled surface shapes, we prepared films without patterns, with a line pattern, and with laterally buckled patterns (B1 and B2) with the same film thickness (1.75 mm) and measured the stress relaxation curves by using a texture analyzer (TXA^{TM} texture analyzer, Yeonjin S-Tech) [49,50]. We compressed the films with a flat probe to a 10% strain based on the film thickness, maintained the pressure for 60 s, and measured the change in stress with time. As shown in Fig. 5D, the maximum stress on the flat film was 0.215 MPa, and the stress on the film with line patterns was reduced to 0.162 MPa. Interestingly, the stress on the film with laterally buckled structures (0.126 MPa) was much smaller than that on the film with the line patterns. A finite element method (FEM) simulation was conducted to compare the kinetic energy transferred through the films with line shapes and laterally buckled shapes. When we measured the kinetic energy on the bottom of the films, we found that the bottom of the laterally buckled shapes transferred less energy than did the bottom of the line shapes (Fig. 5E). The design and the simulation results can be seen in the supporting information (Fig. S15).

3. Conclusion

We have presented a scheme of function transformation of a film through shape morphing of straight lines and rectangular shapes on the surface of the film. Through shape transformation from a line to a laterally buckled shape, normal stress can be dissipated due to spring deformation. Additionally, an inversely tapered shape transformed from a rectangular shape can show oil-repellent functions. For shape transformation, we controlled the water affinity of the liquid prepolymer to keep water molecules within the hydrogel networks during photopolymerization and applied vacuum conditions for easy infiltration of the liquid prepolymer within the swollen hydrogel shapes. Function transformation can be a platform to create unprecedented functions arising from unique shapes morphed from conventional straight shapes.

4. Materials and methods

4.1. Preparation of microtemplates to fabricate hydrogel patterns

First, silicon masters with line/space patterns and square hole structures were prepared by conventional photolithography and dry etching processes. Then, we prepared microtemplates by using PDMS and PFPE. PDMS (Sylgard 184, Dow Corning) prepolymer was mixed with a curing agent at a weight ratio of 10:1. Then, the mixture was

poured onto silicon masters. After crosslinking at 60 °C for more than 12 h, the PDMS mold was peeled off from the master. PFPE (JUNGSUNG polymer Co., Ltd.) was prepared by blending 95 wt% prepolymer with 5 wt% 2-hydroxy-2-methylpropiophenone (Darocur 1173, Sigma–Aldrich). The mixture was dropped onto the prepared square hole masters (silicon or PDMS) with designed surface textures and covered by a PET film, followed by UV exposure for 3 min and 30 s (FusionCure 360–08, 352 nm, 13 W). Subsequently, the crosslinked PFPE was peeled off from the master.

4.2. Preparing the HEMA-co-AAm hydrogels

The hydrogels were prepared using AAm (Sigma, A8887) and 2-hydroxyethyl methacrylate (HEMA; Sigma, 128635) as monomers, N, N-methylenebisacrylamide (MBAA; Sigma, M7279) as a crosslinker, and 2-hydroxy-2-methylpropiophenone (Darocur 1173; Sigma) as a photoinitiator. In a vial, we mixed 3.22 g of HEMA, 0.01 wt% MBAA, 0.1 wt% Darocur 1173 and AAm (0.05 wt% for the swelling ratio of 1.53, 0.09 wt% for the swelling ratio of 1.71, 0.16 wt% for the swelling ratio of 2.01, and 0.32 wt% for the swelling ratio of 2.76) to control the swelling ratio of the hydrogels. The mixtures were stirred by using a magnetic stirrer overnight.

4.3. Fabrication of the re-entrant structures (Figure S1)

The hydrogel mixtures were placed onto prepared PFPE molds (rectangular structures) and covered by a PET film (adhesion promoter coated film; SKC, SH82) followed by UV exposure for 50 s (FusionCure 360–08, wavelength = 352 nm, 13 W). After that, the crosslinked HEMA-co-AAm hydrogel hole structure film was peeled off from the PFPE molds. The prepared rectangular hydrogel hole arrays (spacing S = 100 μm with the same width W = 100 μm and depth D = 50 μm) were swollen in deionized water for 1 h. After swelling, the excess water was removed by a Kimwipe, and a UV-curable polymer was placed onto the swelled hydrogel. The air cavities in the rectangular hydrogel structure were removed in a vacuum chamber. After removing the air cavities, we placed a PET film on the liquid prepolymer and crosslinked the liquid prepolymer by UV exposure for 1 min 30 s (Fusion cure 360–08, wavelength = 352 nm, 13 W). Subsequently, the UV-cured re-entrant structures were peeled off from the swollen hydrogel structures.

4.4. Fabrication of the buckled structures (Fig. S2)

Hydrogel mixtures were placed on PDMS line structures and covered with PET films. The hydrogel prepolymers were cured via UV exposure for 2 min. After that, line-shaped hydrogel structures were peeled off from the PDMS structures. The prepared embossed hydrogel line structure arrays were swollen in deionized water for 1 h. After swelling, the water around the structure was removed by a Kimwipe, and UV-curable prepolymers (PFPE (JUNGSUNG Polymer Co., Ltd.), PUA 301, and PUA 311 (MCNet Co., Ltd.)) were placed on the mold and then covered by PET film. The polymer was cured by UV exposure for 50 s. Subsequently, the inverse structures obtained from the laterally wrinkled structures were peeled off from the swollen hydrogel structures. PS, PDMS or a UV-curable material was placed on the prepared inverse structures and cured by heat or UV exposure. The solidified polymers with the original shapes were peeled off from the mold with the inverse shape.

4.5. Fabrication of PS structures (re-entrant and buckling structures)

A solution of PS (Mw: 2400, Yakuri Pure Chemicals Co., Ltd.) dissolved in toluene (Sigma–Aldrich) was coated onto a silicon wafer substrate. We placed the prepared mold (PDMS or UV-cured polymers) onto the PS-coated substrate and applied pressure (~4 bar), followed by increasing the substrate temperature to 150 °C, which is above the Tg (55 ~ 70 °C) of PS (Mw: 2100 ~ 2850), for 25 min. After that, the mold was peeled off from the PS structures.

Measurement of stress relaxation curves: To measure stress relaxation, we used a texture analyzer (TXATM texture analyzer, Yeonjin S-Tech). The samples were compressed using a flat probe (3 mm diameter) to 10% strain, and pressure was maintained for 1 min. The strain speed was set to 0.1/s, and the change in stress with time was measured.

4.6. FEM simulation

Conventional FEM software (COMSOL, MULTIPHYSICS) was used to obtain the kinetic energy applied on the bottom of the line and buckled structures. We used structural mechanics modules and a physics-controlled mesh. Our design involved cuboids placed on line-shaped and buckled structures to apply uniform normal forces. The applied force was time dependent, and we measured the kinetic energy density of the bottom of the line-shaped and buckled structures.

Declaration of Competing Interest

The authors declare that they have no known competing financial interests or personal relationships that could have appeared to influence the work reported in this paper.

Acknowledgements

This work was financially supported by Seoul National University of Science & Technology.

Appendix A. Supplementary data

Supplementary data to this article can be found online at https://doi.org/10.1016/j.cej.2022.134665.

References

[1] D.-Y. Khang, H. Jiang, Y. Huang, J.A. Rogers, A stretchable form of single-crystal silicon for high-performance electronics on rubber substrates, Science 311 (5758) (2006) 208–212.
[2] Y. Gu, L. Zhang, J.K.W. Yang, S.P. Yeo, C.-W. Qiu, Color generation via subwavelength plasmonic nanostructures, Nanoscale 7 (15) (2015) 6409–6419.
[3] T.‘. Liu, C.-J. Kim, Turning a surface superrepellent even to completely wetting liquids, Science 346 (6213) (2014) 1096–1100.
[4] R. Blossey, Self-cleaning surfaces—virtual realities, Nat. Mater. 2 (5) (2003) 301–306.
[5] B. Bhushan, Biomimetics: lessons from nature–an overview, Phil. Trans. R. Soc. 367 (1893) (2009) 1445–1486.
[6] Y. Zheng, H. Bai, Z. Huang, X. Tian, F.-Q. Nie, Y. Zhao, J. Zhai, L. Jiang, Directional water collection on wetted spider silk, Nature 463 (7281) (2010) 640–643.
[7] J. Ju, H. Bai, Y. Zheng, T. Zhao, R. Fang, L. Jiang, A multi-structural and multi-functional integrated fog collection system in cactus, Nat. Commun. 3 (1) (2012) 1–6.
[8] K.-H. Chu, R. Xiao, E.N. Wang, Uni-directional liquid spreading on asymmetric nanostructured surfaces, Nat. Mater. 9 (5) (2010) 413–417.
[9] B.R. Wasik, S.F. Liew, D.A. Lilien, A.J. Dinwiddie, H. Noh, H. Cao, A. Monteiro, Artificial selection for structural color on butterfly wings and comparison with natural evolution, Proc. Natl. Acad. Sci. 111 (33) (2014) 12109–12114.
[10] S. Jalili-Firoozinezhad, F.S. Gazzaniga, E.L. Calamari, D.M. Camacho, C.W. Fadel, A. Bein, B. Swenor, B. Nestor, M.J. Cronce, A. Tovaglieri, O. Levy, K.E. Gregory, D. T. Breault, J.M.S. Cabral, D.L. Kasper, R. Novak, D.E. Ingber, A complex human gut microbiome cultured in an anaerobic intestine-on-a-chip, Nat. Biomed. Eng. 3 (7) (2019) 520–531.
[11] S. Baik, D.W. Kim, Y. Park, T.-J. Lee, S. Ho Bhang, C. Pang, A wet-tolerant adhesive patch inspired by protuberances in suction cups of octopi, Nature 546 (7658) (2017) 396–400.
[12] H.H. Lee, Fundamentals of microelectronics processing, McGraw-Hill Education, 2018.
[13] D.W. Yee, M.D. Schulz, R.H. Grubbs, J.R. Greer, Functionalized 3D architected materials via thiol-mchael addition and two-photon lithography, Adv. Mater. 29 (16) (2017) 1605293.
[14] D.A. Walker, J.L. Hedrick, C.A. Mirkin, Rapid, large-volume, thermally controlled 3D printing using a mobile liquid interface, Science 366 (6463) (2019) 360–364.
[15] J. Kim, J.A. Hanna, M. Byun, C.D. Santangelo, R.C. Hayward, Designing responsive buckled surfaces by halftone gel lithography, Science 335 (6073) (2012) 1201–1205.

[16] D.H. Kang, S.M. Kim, B. Lee, H. Yoon, K.-Y. Suh, Stimuli-responsive hydrogel patterns for smart microfluidics and microarrays, Analyst 138 (21) (2013) 6230–6242.
[17] B.o. Cao, G. Wu, Y.u. Xia, S. Yang, Buckling into single-handed chiral structures from pH-sensitive hydrogel membranes, Extreme Mech. Lett. 7 (2016) 49–54.
[18] X. Zhu, G. Wu, R. Dong, C.-M. Chen, S. Yang, Capillarity induced instability in responsive hydrogel membranes with periodic hole array, Soft Matter 8 (31) (2012) 8088–8093.
[19] M. Guvendiren, S. Yang, J.A. Burdick, Swelling-induced surface patterns in hydrogels with gradient crosslinking density, Adv. Funct. Mater. 19 (19) (2009) 3038–3045.
[20] J. Kim, J. Yoon, R.C. Hayward, Dynamic display of biomolecular patterns through an elastic creasing instability of stimuli-responsive hydrogels, Nat. Mater. 9 (2010) 159–164.
[21] Z. Ji, C. Yan, B.o. Yu, X. Zhang, M. Cai, X. Jia, X. Wang, F. Zhou, 3D Printing of hydrogel architectures with complex and controllable shape deformation, Adv. Mater. Technol. 4 (4) (2019) 1800713, https://doi.org/10.1002/admt.v4.410.1002/admt.201800713.
[22] O. Fourmann, M.K. Hausmann, A. Neels, M. Schubert, G. Nystrom, T. Zimmermann, G. Siqueira, 3D printing of shape-morphing and antibacterial anisotropic nanocellulose hydrogels, Carbohydr. Polym. 259 (2021), 117716.
[23] A. Nojoomi, H. Arslan, K. Lee, K. Yum, Bioinspired 3D structures with programmable morphologies and motions, Nat. Commun. 9 (2018) 3705.
[24] Z.J. Wang, C.N. Zhu, W. Hong, Z.L. Wu, Q. Zheng, Cooperative deformations of periodically patterned hydrogels, Sci. Adv. 3 (9) (2017), https://doi.org/10.1126/sciadv.1700348.
[25] X. Zhu, S. Wu, C. Yang, H. Deng, Y. Du, X. Shi, Electrical writing to three-dimensional pattern dynamic polysaccharide hydrogel for programmable shape deformation, Macromol. Rapid. Commun. 42 (2021) 2000342.
[26] Z. Xu, J. Fu, Programmable and reversible 3D-/4D-shape-morphing hydrogels with precisely defined ion coordination, ACS Appl. Mater. Interfaces 12 (23) (2020) 26476–26484.
[27] H. Zhang, X. Guo, J. Wu, D. Fang, Y. Zhang, Soft mechanical metamaterials with unusual swelling behavior and tunable stress-strain fcurves, Sci. Adv. 4 (2018) eaar8535.
[28] Z. Jiang, B. Diggle, I.C.G. Shackleford, L.A. Connal, Tough, self-healing hydrogels capable of ultrafast shape changing, Adv. Mater. 31 (2019) 1904956.
[29] C. Wang, K. Hu, C. Zhao, Y. Zou, Y. Liu, X. Qu, D. Jiang, Z. Li, M.-R. Zhang, Z. Li, Customization of conductive elastomer based on PVA/PEI for stretchable sensors, Small 16 (2020) 1904758.
[30] X. Qu, X. Ma, B. Shi, H. Li, L. Zheng, C. Wang, Z. Liu, Y. Fan, X. Chen, Z. Li, Z. L. Wang, Refreshable braille display system based on triboelectric nanogenerator and dielectric elastomer, Adv. Funct. Mater. 31 (2021) 2006612.
[31] V.R. Tirumala, C.M. Stafford, L.E. Ocola, J.F. Douglas, L. Mahadevan, Geometric control of rippling in supported polymer nanolines, NANOLett. 12 (3) (2012) 1516–1521.
[32] R. Jiang, J. Xiao, J. Song, Buckling of thin gel strip under swelling, Theor. Appl. Mech. Lett. 7 (3) (2017) 134–137.
[33] P. Nardinocchi, E. Puntel, Swelling-induced wrinkling in layered gel beams, Proc. R. Soc. A 473 (2207) (2017) 20170454, https://doi.org/10.1098/rspa.2017.0454.
[34] G. Lin, D. Ge, Y. Tang, Y.u. Xia, G. Wu, L. Han, S. Yang, J. Yin, Cuts guided deterministic buckling in arrays of soft parallel plates for multifunctionality, ACS Appl. Mater. Interfaces 9 (34) (2017) 29345–29354.
[35] H. Lee, J.G. Bae, W.B. Lee, H. Yoon, Mechano-responsive lateral buckling of miniaturized beams standing on flexible substrates, Soft Matter 13 (45) (2017) 8357–8361.
[36] H. Yoon, A. Ghosh, J.Y. Han, S.H. Sung, W.B. Lee, K. Char, Lateral Buckling of High Aspect Ratio Janus Nanowalls, Adv. Funct. Mater. 22 (17) (2012) 3723–3728.
[37] C.N. LaFratta, L. Li, J.T. Fourkas, Soft-lithographic replication of 3D microstructures with closed loops, Proc. Natl. Acad. Sci. 103 (23) (2006) 8589–8594.
[38] S.-J. Choi, P.J. Yoo, S.J. Baek, T.W. Kim, H.H. Lee, An ultraviolet-curable mold for sub-100-nm lithography, J. Am. Chem. Soc. 126 (25) (2004) 7744–7745.
[39] S.-J. Choi, H.N. Kim, W.G. Bae, K.-Y. Suh, Modulus-and surface energy-tunable ultraviolet-curable polyurethane acrylate: properties and applications, J. Mater. Chem. 21 (38) (2011) 14325–14335.
[40] T. Kim, H. Yoon, H.-J. Song, N. Haberkorn, Y. Cho, S.H. Sung, C.H. Lee, K. Char, P. Theato, Toward mass producible ordered bulk heterojunction organic photovoltaic devices, Macromol. Rapid Commun. 33 (23) (2012) 2035–2040.
[41] J. Kim, Y. Ryu, C.H. Kim, S.G. Heo, K.-Y. Yoo, H. Yoon, Robust superomniphobic micro-hyperbola structures formed by capillary wrapping of a photocurable liquid around micropillars, Adv. Funct. Mater. 31 (18) (2021) 2010053, https://doi.org/10.1002/adfm.v31.1810.1002/adfm.202010053.
[42] J. Rhee, J. Park, S. Kwon, H. Yoon, H.H. Lee, Fabrication of reversely tapered three-dimensional structures and their application to organic light-emitting diodes, Adv. Mater. 15 (13) (2003) 1075–1078.
[43] R. Hensel, R. Helbig, S. Aland, H.-G. Braun, A. Voigt, C. Neinhuis, C. Werner, Wetting resistance at its topographical limit: the benefit of mushroom and serif T structures, Langmuir 29 (4) (2013) 1100–1112.
[44] A. Tuteja, W. Choi, G.H. McKinley, R.E. Cohen, M.F. Rubner, Design parameters for superhydrophobicity and superoleophobicity, MRS Bull. 33 (8) (2008) 752–758.
[45] A. Tuteja, W. Choi, M. Ma, J.M. Mabry, S.A. Mazzella, G.C. Rutledge, G. H. McKinley, R.E. Cohen, Designing superoleophobic surfaces, Science 318 (5856) (2007) 1618–1622.
[46] L. Chen, Z. Guo, W. Liu, Outmatching superhydrophobicity: bio-inspired re-entrant curvature for mighty superamphiphobicity in air, J. Mater. Chem. A 5 (28) (2017) 14480–14507.
[47] S.Y. Lee, Y. Rahmawan, S. Yang, Transparent and superamphiphobic surfaces from mushroom-like micropillar arrays, ACS Appl. Mater. Interfaces 7 (43) (2015) 24197–24203.
[48] J.-H. Back, D. Baek, J.-W. Park, H.-J. Kim, J.-Y. Jang, S.-J. Lee, Shock absorption of semi-interpenetrating network acrylic pressure-sensitive adhesive for mobile display impact resistance, Int. J. Adhes. Adhes. 99 (2020), 102558.
[49] H. Singh, A. Rockall, C.R. Martin, O.K. Chung, G.L. Lookhart, The analysis of stress relaxation data of some viscoelastic foods using a texture analyzer, J. Texture Stud. 37 (4) (2006) 383–392.
[50] S. Krödel, L. Li, A. Constantinescu, C. Daraio, Stress relaxation in polymeric microlattice materials, Mat. Des. 130 (2017) 433–441.